Tanzania Journal of Engineering and Technology 2025, **44**(2):106-116
OPEN ACCESS articles distributed under Creative Commons Attribution Licence [CC BY-ND]
Websites: https://ajol.org/tjet; https://tjet.udsm.ac.tz

ISSN 1821-536X (**print**); ISSN 2619-8789 (**electronic**)
https://doi.org/10.52339/tjet.v44i2.1271

Special Issue – 8th International Conference on Mechanical and Industrial Engineering, October 24 – 25, 2024 at The Nelson Mandela African Institute of Science and Technology, Arusha - Tanzania

Optimizing the Processing Temperature for Synthesis of Silver Nanoparticles within Cellulose-Wool Keratin supramolecular Matrix using Butylmethylimmidazolium Chloride Ionic Liquid

Ngesa Ezekiel Mushi

Department of Mechanical and Industrial Engineering, College of Engineering and Technology, University of Dar es Salaam, P.O Box 35131, Dar es Salaam, Tanzania.

Corresponding Author: mushi.ngesa@udsm.ac.tz; ORCID: 0009-0000-5625-186X

ABSTRACT

To date, the synthesis of silver nanoparticles on the surface of cellulose and wool keratin biopolymer, while dissolved in ionic liquid, is attractive because of its biomedical potential. However, the optimal processing temperature for the nanoparticle formation is unclear. The previously reported temperature of approximately 120°C gives unpredictable results. The current study employs a combination of 50% cellulose and 50% keratin, along with 69 mg of silver chloride, in Butylmethylimidazolium Chloride BMImCl ionic liquid, using a single-pot process to produce a supramolecular film via non-derivatized mechanochemical interactions. The primary objective is to experimentally establish the processing temperature to achieve stable growth of metallic silver nanoparticles. The synthesis was conducted by heating the ionic mixture at temperatures of 110°C, 120°C, and 130°C. The study observed that raising the temperature to around 130ºC for 5 min is more practical. Moreover, though this data is higher, it does not compromise the thermal stability of cellulose and keratin's structure. The structural properties of the nanoparticles have been confirmed using Fourier transform spectroscopy (FTIR) and scanning electron microscopy (SEM). Furthermore, energy-dispersive X-ray spectroscopy (EDS) and powder X-ray diffraction (XRD) provide valuable insights into the physical characteristics of the produced silver nanoparticles, with a diameter of around 8.5 nm, and are uniformly distributed in-plane within the matrix. While the underlying mechanisms remain uncertain, they likely involve anchoring ionic silver onto the wool keratin while dissolved within the ionic liquid at elevated temperatures before reducing to metallic silver at room temperatures. Besides being sustainable, this green approach enhances understanding of the possibility of creating stable silver nanoparticles within the supramolecular matrix, which is essential for future applications in the biomedical field.

ARTICLE INFO

1st Submitted: **Apr. 23, 2024**

Presented: **Oct. 24, 2024**

Revised: **Nov. 26, 2024**

Accepted: **Jan, 30, 2025**

Published: **June, 2025**

Keywords: *Wool, keratin, cellulose, silver nanoparticles, supramolecular film, 1-Butyl-3-methylimidazolium chloride.*

INTRODUCTION

Metallic nanoparticles are highly appealing for various technological applications due to their unique optical, plasmonic, quantum, and biomedical properties. Among these, silver nanoparticles are particularly interesting, even more so than gold. Their biomedical features are especially noteworthy, as silver nanoparticles exhibit both antiviral and antibacterial effects against gram-negative and gram-positive bacteria while demonstrating biocompatibility (Wei et al., 2015, Tran et al., 2016). The synthesis of silver nanoparticles can be achieved through several methods, including both chemical and biological approaches, among other alternatives. However, the synthesis process is complex. Commonly used chemicals, such as formaldehyde and ethylene glycol (Vishwanath and Negi, 2021), can pose toxicity risks. Furthermore, silver is versatile and can exist in ionic, metallic, or compound-based forms. Concerns about using silver cations and silver-based compounds have been raised due to potential impacts on human health and aquatic life (Galazzi et al., 2019). Generally, silver is unreactive at room temperature because of its filled 4d valence shell. Its unique monovalent atomic configuration contributes to its distinct characteristics. Maintaining the properties of the metallic silver nanoparticles is crucial, and their size and morphology play vital roles.

Cellulose, in its simplest form, consists of β-1,4 linked glucan chains. Hydrogen bonds form between hydroxyl groups and oxygen atoms within a single glucose chain, and its neighboring chains maintain an extended polymer conformation. Together with van der Waals forces, hydrogen bonding helps to arrange glucan chains side by side, promoting the parallel stacking of cellulose microfibrils into crystalline cellulose (Somerville, 2006, Taylor, 2008). The natural form of crystalline cellulose is known as cellulose I. This form can be irreversibly converted into cellulose II, also termed regenerative cellulose, which is more stable than cellulose I (Kobayashi et al., 2011). All organisms that synthesize cellulose, including bacteria, algae, tunicates, and higher plants, possess cellulose synthase proteins that catalyze the polymerization and crystallization of glucan chains (Saxena et al., 2001). In contrast, keratins are a group of cysteine-rich fibrous proteins. The synthesis of α-keratin begins near focal adhesions on the cell membrane (Wang et al., 2016). Once the cell has been filled with the correct keratin and structured appropriately, it undergoes keratin stabilization and eventually dies (Wang et al., 2016). These fully developed α-keratin cells are the main components of hair, sheep wool, chicken feathers, the outer layer of nails and horns, and the epidermal layer of the skin (Eckhart et al., 2013).

Cellulose serves as a reinforcing material, while keratin possesses antimicrobial properties and various biological activities. This dual function enables the conversion of animal waste into valuable products. For example, previous studies have demonstrated the practicality of combining wool keratin and cellulose, resulting in a supramolecular film that overcomes the mechanical challenges of producing a strong film of pure wool keratin (Tran et al., 2016). Data from Fourier transform infrared (FTIR) spectroscopy, combined with partial least-squares regression, indicate no chemical alteration in the structures, confirming the successful regeneration of cellulose and keratin (Mushi, 2023).

Various studies have demonstrated the potential of the bottom-up approach in anchoring metallic nanoparticles or their oxides, with the specific protocols varying accordingly (Kumari et al., 2023). For instance, cobalt magnetic nanoparticles can be grown onto the surface of carboxylated cellulose nanofibrils (El Idrissi et al., 2022, Galland et al., 2013), copper oxide nanoparticles can be synthesized on cellulose (Shao et al., 2016, Tran et al.,

2017), and gold nanoparticles can also be anchored onto cellulose (Doghish et al., 2022). Similarly, silver oxide nanoparticles have promising implications (Lopez-Carrizales et al., 2022). In conventional processes, nanoparticles often face coagulation and aggregation within colloidal suspensions. Metallic silver is no exception. The bottom-up approach for synthesizing silver nanoparticles offers a unique way to control stability in colloidal suspensions, which is difficult to overcome traditionally. Conversely, bulk silver features a densely packed structure. It exhibits a face-centered cubic crystal structure akin to solid metals like steel or copper. While this structure is stable, its properties may not always be desirable because of the structural limitations, i.e., size and morphology (Xia et al., 2012). Consequently, top-down approaches for producing metallic silver nanoparticles may be impractical. Additionally, unlike bulk structures, these nanoparticles can easily oxidize in the presence of light, which does not make economic sense.

In the bottom-up approach, the nucleation of metal nanoparticles is crucial for their growth stage during the reduction process. One of them is homogeneous distribution and size. Another is that nanoscale functionalities can be expressed more effectively in microscale structures. Various synthetic polymers and biopolymers have been used to encapsulate these nanoparticles. For example, silver nanoparticles have been anchored to methacrylic acid copolymer beads (Gangadharan et al., 2010). Once nucleated, stable nanoparticles are anchored on the biopolymer surface and maintained in solid films. Hydroxyl or carboxylic groups, vital nucleation sites, are significant in this process. Silver nanoparticles can be synthesized using suitable reaction environments, including fruit juices (Singh et al., 2024, Jemal et al., 2017), organic solvents (Vishwanath and Negi, 2021), or ionic liquids (Tran et al., 2016). Following the non-derivatized mechanochemical method, synthesis occurs within dissolved cellulose and wool keratin in an ionic liquid (Mushi, 2023, Tran et al., 2016). This approach aims to grow the nanoparticles on cellulose or wool keratin surfaces, effectively stabilizing the silver nanoparticles. Successful synthesis depends on several parameters, including processing temperature, cellulose, keratin, compound-based silver solubility in ionic liquid, reducing reagents, washing techniques, or exposure to light. Primarily, light absorption at 400 nm distinguishes the presence of metallic silver, while a characteristic peak around 48° 2θ confirms the presence of metallic silver nanoparticles from other metallic crystal structures (Tran et al., 2016). In contrast, silver oxide nanoparticles appear at approximately 32° 2θ. Previously, it was demonstrated that introducing silver salt into the cellulose-wool (celwool) supramolecular film during the dissolution of cellulose and keratin in 1-Butyl-3-Methylimidazolium Chloride (BMImCl) reduces silver ions to metallic silver within the film (Tran et al., 2016). The high temperature used in this process is around 120°C, which is safe and does not compromise the thermal stability of cellulose, wool keratin, or the ionic liquid. Although ionic liquids have low melting points and can tolerate much higher temperatures (Dharaskar et al., 2013), the optimal temperature for achieving a stable structure is still unclear. The structural properties of silver nanoparticles were challenging to predict. Specifically, the thermal stability limits of the ionic liquid, cellulose, and keratin related to silver nanoparticle formation have not yet been established, highlighting the gaps in this research.

As it is well established, converting silver ions or compound-based silver into their metallic nanoparticle form offers significant advantages in increasing their functionality, environmental remediation, and commercial application. To meet stringent measures for biomedical

applications, an efficient approach was established, as explained, based on cellulose, keratin, and ionic liquid, which is sustainable and greener. Compared to conventional methods, the benefits and challenges of the technique have been extensively discussed in previous studies (Gangadharan et al., 2010, Tran et al., 2016). The developed cellulose-wool-silver (Agcelwool) supramolecular films can effectively maintain the size and morphology of silver nanoparticles. The difficulties in predicting the structural properties of the silver nanoparticle remained to be addressed. The current work emphasizes the importance of temperature as a processing parameter in the synthesis, particularly regarding the optimal conditions for the nucleation and growth of silver nanoparticles within cellulose-keratin films. The potential of using cellulose and keratin to grow silver nanoparticles presents a promising opportunity to utilize ionic liquids while emphasizing their role as greener solvents. This approach is particularly relevant for applications in the biomedical field, which remains a captivating area for research and innovation.

EXPERIMENTAL METHOD

Materials

Microcrystalline cellulose (MCC) with DP ≈ 300, Sodium Borohydride ($NaBH_4$), and Silver Chloride (AgCl) were from Sigma-Aldrich and were used as received. Raw (untreated) sheep wool, obtained from a local farm in Milwaukee, USA, was cleaned by Soxhlet extraction using a 1:1 (v/v) acetone/ethanol mixture at 80°C for 48 hrs. The wool, rich in α-keratin structure, was then rinsed with distilled water and dried at 100°C for 12 hrs. 1-Methylimidazole and n-chlorobutane (both from Alfa Aesar, Ward Hill, MA) were distilled and subsequently used to synthesize BMImCl using a method previously reported (Rosewald et al., 2014).

Procedure for synthesis of silver nanoparticles celwool film in BMImCl liquid

Silver nanoparticles were synthesized following the previously developed procedure for synthesizing celwool films (Tran et al., 2016). The preparation protocol is displayed in the flow chart Figure 1. First, the wool was dissolved in BMImCl at 120°C. Once dissolved, the solution temperature was reduced to 90°C. Second, the MCC powder was added to the wool/BMImCl solution, resulting in a 5050 cellulose-to-wool composition. Third, in a separate flask, AgCl, in the weight of 69 or 138 mg, was dissolved in 2 mL of BMImCl, and the mixture was then added dropwise to the BMImCl solution of cellulose and wool. The resulting solution was then cast onto poly(tetrafluoroethylene) (PTFE) molds with the desired thickness on Mylar films to produce a wet ionic gel. Pure cellulose and 5050celwool films were prepared as reference materials. The ionic gels were then kept in the dark and at room temperature for 24 hrs to allow gelation to yield gel films. The gel films between two PTFE meshes were placed in an aqueous solution of $NaBH_4$ in the dark at room temperature for 48 hrs to reduce silver ions to metallic silver nanoparticles. Subsequently, the reduced film was washed and dried in an oven at 40°C under pressure between filter membranes overnight to yield the solid supramolecular films.

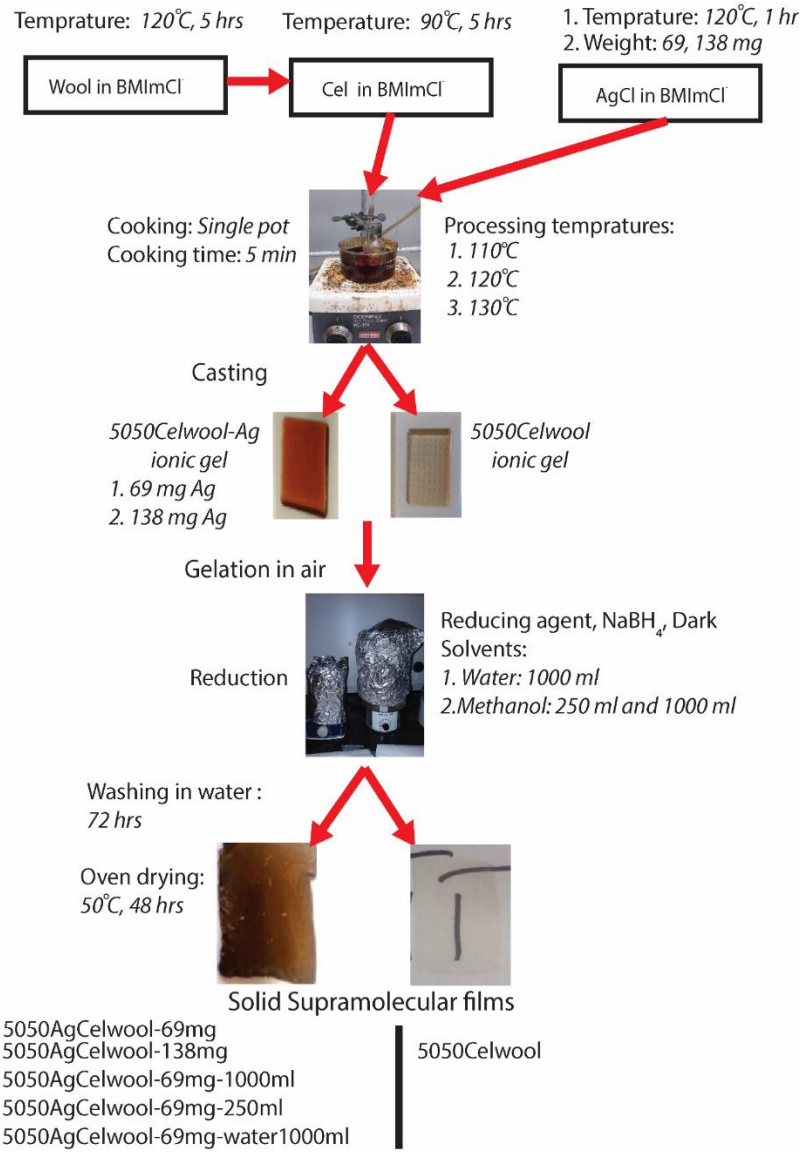

Fig.1: Schematic flow chart of silver nanoparticle synthesis within the celwool supramolecular film using BMImCl ionic liquid solution.

Characterization techniques

Fourier Transform Infrared Spectroscopy (FTIR) spectra (from 450 to 4000 cm^{-1}) were recorded on a Spectrum 100 series FTIR spectrometer (PerkinElmer, USA) at 2 cm^{-1} resolution by the KBr method. Each spectrum was an average of 64 individual spectra. X-ray diffraction (XRD) measurements were taken on a Rigaku MiniFlex II diffractometer utilizing nickel-filtered Cu Kα radiation (1.54059 Å). The voltage and current of the X-ray tube were 30 kV and 15 mA, respectively. The samples were measured within the 2θ angle range from 2 to 40°. The scan rate was 5°/min. Data processing procedures were performed with the Jade 8 program package. The surface and cross-sectional morphologies of the films were examined under a vacuum with a JEOL JSM-6510LV/LGS scanning electron microscope (SEM) with standard secondary electron (SEI) and backscattering electron (BEI) detectors. The SEM is equipped with an Energy Dispersion X-ray detector for chemical composition imaging and mapping. Before scanning electron microscopy (SEM) examination, the film specimens were made conductive by applying a 20 nm gold-palladium coating to their surfaces using an

Emitech K575x Peltier-cooled sputter coater (EMI-Tech Products, Timpson, TX).

RESULTS AND DISCUSSION

Optimization of processing temperature for synthesis of silver nanoparticles

As presented in Figure 1, the optimization process for synthesizing silver nanoparticles is clarified. Increasing the temperature may cause damage or "denature" the protein structure, but cellulose and the ionic liquid can remain stable. This is true since the thermal stability is around 170°C (Brebu and Spiridon, 2011), while cellulose and BMImCl may reach 275°C (Fukuzumi et al., 2010) and 246°C (Dharaskar et al., 2013), respectively. Cellulose dissolves at 90°C, while wool dissolves at around 120°C in the BMImCl solution. In the current study, wool was dissolved first. Then, cellulose was dissolved in an ionic mixture in the presence of wool. The low molecular weight and density of the wool keratin biopolymer of wool supports this. Low molecular weight increases dispersibility. Following wool dissolution, the temperature is lowered to accommodate cellulose. The BMImCl solution contains approximately 6 wt% cellulose and wool in a 50 by 50 percent composition, the highest solubility for this material (Mushi, 2023), forming a supramolecular structure. Complete dissolution is accomplished after intense mixing at elevated temperatures to break down the macromolecular bonding. The dissolution of AgCl was performed in a fresh ionic liquid, where a temperature of 120°C was maintained for at least 20 minutes with vigorous stirring. The previous studies maintained the ionic solution containing silver ions and the supramolecular solution at 120°C (Tran et al., 2016). Likewise, the 5050celwool solution, as a reference material, was mixed at this temperature for 20 minutes as a reference. For optimization, in addition to 120°C, the ionic solution of 5050Agcelwool was processed at 110°C and a higher temperature of 130°C, with no noticeable differences observed during visual inspection. For mixing at higher temperatures, the procedure involves an initial mixing at 120°C for 20 minutes, followed by a gradual increase in temperature for 5 min to preserve the regenerative structure of cellulose and keratin. The casting process, where the mixture is poured into a mold to form a film, is carried out immediately while the mixture is still hot. FTIR analysis provides a comprehensive understanding of the supramolecular films to evaluate the effect of the processing conditions at elevated temperatures. Figure 2 displays a clear spectrum of the supramolecular films. The red line represents the 5050celwool films, while the spectrum for the 5050Agcelwool films, prepared at 130°C, is presented as a black curve. Previous studies confirmed the regeneration of cellulose and keratin, at least after 120°C processing temperature (Mushi, 2023, Rosewald et al., 2014, Tran et al., 2016). As expected, the bands in the 1700–1600 cm^{-1} and 1550 cm^{-1} correspond to the C═O stretch from amide I and the C–N stretch from amide II vibrations. The bands between 1300 and 1200 cm^{-1} arise from the combination of N–H bending and C–N stretching vibrations based on amide III. The significant bands between 1200 and 900 cm^{-1} are due to sugar ring deformations within the cellulose chain. Careful analysis of the 5050celwool spectrum shows no differences from the 5050Agcelwool film. For the optimized study, the data implies a weak interaction exists between the silver nanoparticles and the C═O groups from amide I. Furthermore, minor differences in the amide II region can be observed around 1450 cm^{-1}. The reduction in the intensity of the amide II band in the 5050Agcelwool film could probably be correlated to some interaction between the silver nanoparticles and the amide groups from keratin. Additionally, the peak shifts at approximately 2800 and 3500 cm^{-1} suggest interference in hydrogen bonding within

the 5050Agcelwool film. Technically, these are critical observations, implying that silver nanoparticles are probably predominantly anchored on wool keratin rather than cellulose.

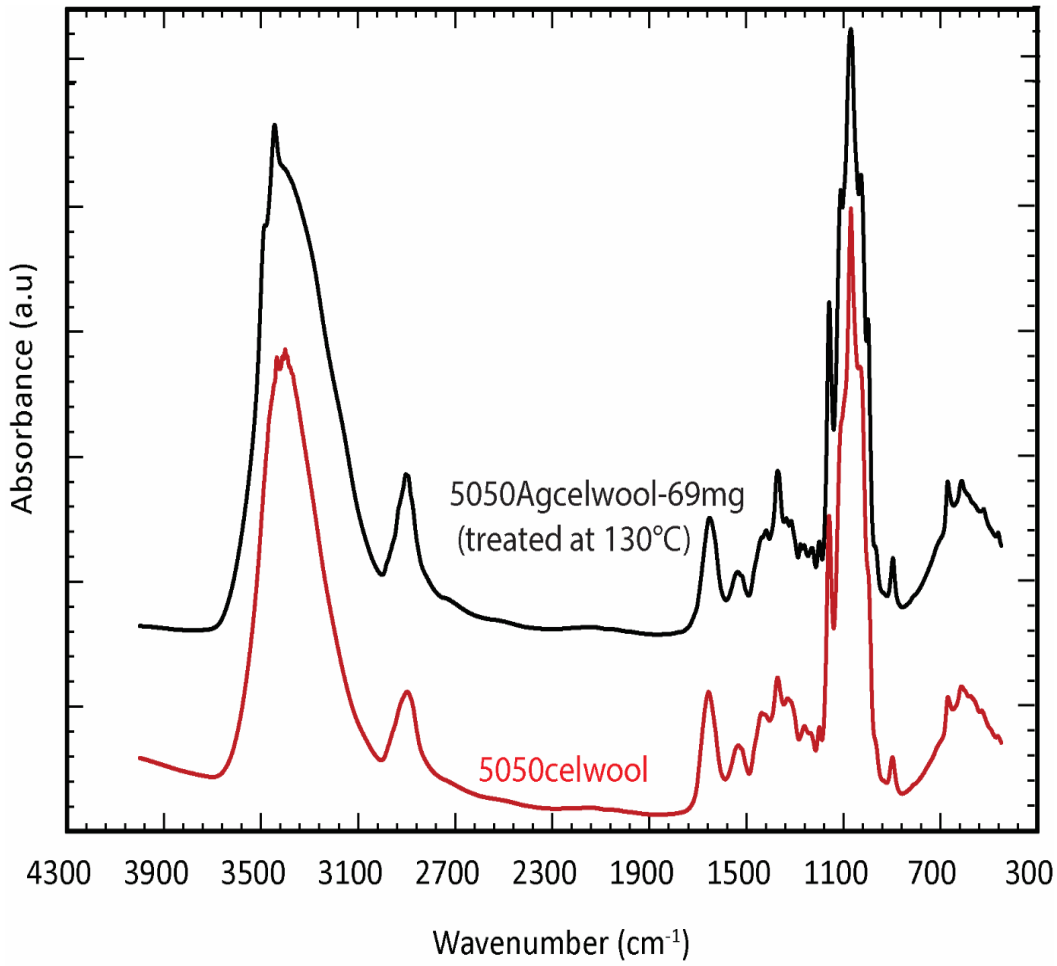

Fig. 2: FTIR spectrum of 5050Agcelwool supramolecular film and the reference material from 5050celwool film.

X-ray diffraction pattern of the 5050Agcelwool supramolecular film

The X-ray diffractograms of 5050Agcelwool, prepared under various conditions, and reference materials from 5050celwool and 5050celchitosan, as shown in Figure 3, reveal essential observations. The presence of regenerated cellulose and wool keratin in the films and the reference materials is expected to produce spectra with two broad bands around $2\theta = 10.75°$ and 20.85°. In contrast, the diffractograms for the 5050Agcelwool film exhibit peaks at 38.47°, 44.57°, 64.87°, and 77.66°. These peaks are attributed to the bands of metallic silver nanoparticles (Tran et al., 2016, Jemal et al., 2017), which is crucial for optimizing the preparation process. The corresponding crystal planes identified are (111), (200), (220), and (311). A sharp crystalline peak and a fingerprint spectrum for metallic silver are anticipated at the (111) plane from the 5050Agcelwool films. The peak for the 5050Agcelchitosan film appears broader. For films reduced in 250 ml of methanol or water using $NaBH_4$ and those processed under optimized conditions at 110°C and 120°C, a weak diffraction peak is observed at the (111) plane. In contrast, the films treated at 130°C significantly increased peak intensity. The extracted data (highlighted in pink) indicates that the diffraction peak heights of the

5050Agcelwool films correspond to the optimized processing conditions, revealing a notable increase at elevated temperatures. This observation represents a potential breakthrough in predicting the formation of silver nanoparticles within the supramolecular film. Although the physical implications of this data remain unclear, further investigation may be needed to improve our understanding of this phenomenon. While nucleation and growth are critical, this study has not investigated them. LaMer burst nucleation, Finke-Watzky, Ostwald ripening, coalescence, or autocatalytic models elucidate the nucleation and growth of silver nanoparticles (Thanh et al., 2014). Based on these models, the critical free energy for nucleation is governed by the Boltzmann reaction kinetics, which, importantly, is a temperature-dependent process. As such, it complements the XRD and FTIR data, suggesting that higher temperature is vital in anchoring metallic silver or silver ions to the biopolymer surface, making the synthesis process possible and more effective or the synthesis protocol more reliable and with predictable results.

The Scherrer equation (see Eq. 1) was used to determine the nanoparticle size in the films, relying on the full width at half-maximum (FWHM) of the XRD peaks (Tran et al., 2016). From peaks 3 and 4 (highlighted pink), the approximate nanoparticle was found to be 8.5 nm, which is significant, as it falls within a range that exhibits unique biomedical properties due to the size effect.

$$\tau = \frac{k\lambda}{\beta cos\theta} \quad (1)$$

Where τ is the nanoparticle size, λ is the X-ray wavelength (nm), and k is a constant (Langford and Wilson, 1978, Fatimah et al., 2022).

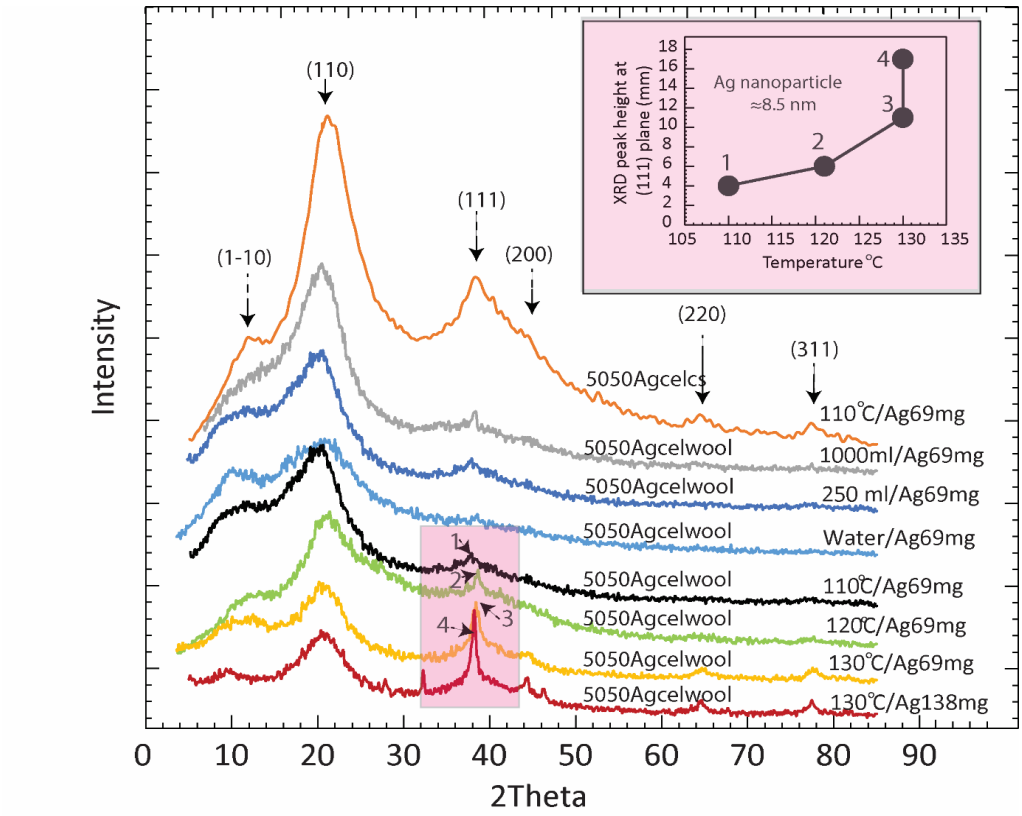

Fig. 3: X-ray diffraction spectrum of the supramolecular films under various preparation conditions and the reference material from 5050celchitosan. The inserted extract (highlighted pink) presents the correlation peak height of the supramolecular films prepared under different processing temperatures for optimization.

SEM topographical images of 5050Agcelwool supramolecular film

The topographical properties of the 5050Agcelwool film were examined to determine the distribution of metallic silver nanoparticles within the supramolecular matrix. Figure 4(a) shows a pure regenerated cellulose film, while Figure 4(b) displays the 5050celwool film. Cellulose typically has a smooth surface. However, the inclusion of wool keratin in the film results in a rough and porous structure with a three-dimensional interconnection throughout. As anticipated, the images of the film align with those previously published for the 5050celwool films (Mushi, 2023). Figure 4(c) provides the topographical image of the 5050Agcelwool film. An EDS image illustrating the distribution of metallic silver on the film is included as an insert. See Figure 4(d). Figure 4(e) offers a cross-sectional view of the fracture surface of the 5050Agcelwool film. From the data in Figure 4(d), it can be inferred that the metallic silver is distributed homogeneously. Moreover, Figure 4(e) reveals a layered structure in which the nanoparticles are dispersed within the plane of the film. Additional information regarding the chemical composition and homogeneity of the film is presented in the energy curve shown in Figure 4(f), which depicts the spectrum obtained under an EDS detector specifically set for carbon (C), hydrogen (H), oxygen (O), and silver (Ag). The presence of aluminum (Al) may have resulted from contamination. Overall, it is clear that the silver nanoparticles are well integrated into the films, appearing as well-distributed nanoparticles throughout

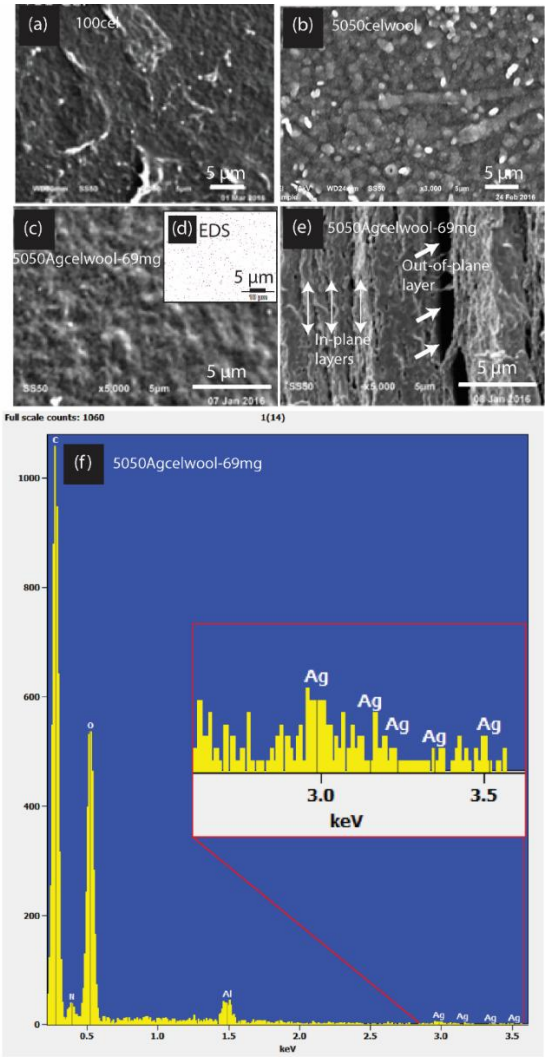

Fig. 4: SEM images of (a) 100cel film (b) 5050celwool film (c) supramolecular film of 5050Agcelwool film (d) EDS image mapping the distribution of metallic silver on the film surface (e) cross-sectional view of the 5050Agcelwool fracture surface (f) EDS spectrum demonstrating the surface composition of the 5050Agcelwool film.

CONCLUSIONS

The current study presents an optimized temperature for synthesizing the silver nanoparticle within the supramolecular matrix containing 50% cellulose and 50% keratin. BMImCl was used as the sole solvent in a single-pot process. By raising the temperature of the ionic mixture to 130°C for 5 min, the silver ions were wholly converted to silver nanoparticles following reduction using $NaBH_4$. The FTIR and XRD data confirm that cellulose and wool keratin remain chemically intact, clearly demonstrating that the regenerative properties of the cellulose and wool keratin were maintained. Moreover, the SEM images showed a supramolecular structure with keratin, cellulose, and silver

nanoparticles homogeneously distributed in the film plane. The silver nanoparticles with sizes of 8.5 nm were estimated, which is essential in biomedical applications. Given the nanoparticle predictability and the reliability of the process, these data could play a substantial role in promoting this green approach through the bottom-up technique.

ACKNOWLEDGMENT

The author is grateful to Marquette University for a postdoctoral fellowship supporting his time doing the research, specifically thanks to Prof Chieu Tran.

REFERENCES

Brebu M. and Spiridon I. (2011). Thermal degradation of keratin waste, *Journal of Analytical and Applied Pyrolysis*, 91: 288-295.

Dharaskar S.A., Wasewar K.L., Varma M.N., Shende D.Z. and Yoo C.K. (2013). Deep removal of sulfur from model liquid fuels using 1-butyl-3-methylimidazolium chloride, *Procedia Engineering*, 51: 416-422.

Doghish A.S., Hashem A.H., Shehabeldine A.M., Sallam A.-A.M., El-sayyad G.S. and Salem S.S. (2022). Nanocomposite based on gold nanoparticles and carboxymethyl cellulose: synthesis, characterization, antimicrobial, and anticancer activities, *Journal of Drug Delivery Science and Technology*, 77: 103874.

Eckhart L., Lippens S., Tschachler E. and Declercq W. (2013). Cell death by cornification, *Biochimica et Biophysica Acta (BBA)-Molecular Cell Research*, 1833: 3471-3480.

El idrissi N., Belachemi L., Merle N., Zinck P. and Kaddami H. (2022). Comprehensive preparation and catalytic activities of Co/TEMPO-cellulose nanocomposites: A promising green catalyst, *Carbohydrate Polymers*, 295: 119765.

Fatimah S., Ragadhita R., Al husaeni D.F. and Nandiyanto A.B.D. (2022). How to calculate crystallite size from x-ray diffraction (XRD) using Scherrer method, *ASEAN Journal of Science and Engineering*, 2: 65-76.

Fukuzumi H., Saito T., Okita Y. and Isogai A. (2010). Thermal stabilization of TEMPO-oxidized cellulose, *Polymer Degradation and Stability*, 95: 1502-1508.

Galazzi R.M., Júnior C.A.L., De lima T.B., Gozzo F.C. and Arruda M.A.Z. (2019). Evaluation of some effects on plant metabolism through proteins and enzymes in transgenic and non-transgenic soybeans after cultivation with silver nanoparticles, *Journal of Proteomics*, 191: 88-106.

Galland S., Andersson R.L., Salajková M., Ström V., Olsson R.T. and Berglund L.A. (2013). Cellulose nanofibers decorated with magnetic nanoparticles–synthesis, structure and use in magnetized high toughness membranes for a prototype loudspeaker, *Journal of Materials Chemistry C*, 1: 7963-7972.

Gangadharan D., Harshvardan K., Gnanasekar G., Dixit D., Popat K.M. and Anand P.S. (2010). Polymeric microspheres containing silver nanoparticles as a bactericidal agent for water disinfection, *Water Research*, 44: 5481-5487.

Jemal K., Sandeep B. and Pola S. (2017). Synthesis, characterization, and evaluation of the antibacterial activity of Allophylus serratus leaf and leaf derived callus extracts mediated silver nanoparticles, *Journal of Nanomaterials*, 2017: 4213275.

Kobayashi K., Kimura S., Togawa E. and Wada M. (2011). Crystal transition from cellulose II hydrate to cellulose II, *Carbohydrate Polymers*, 86: 975-981.

Kumari S., Raturi S., Kulshrestha S., Chauhan K., Dhingra S., András K., Thu K., Khargotra R. and Singh T. (2023). A comprehensive review on various techniques used for synthesizing nanoparticles, *Journal of Materials Research and Technology*, 27: 1739-1763.

Langford J.I. and Wilson A. (1978). Scherrer after sixty years: a survey and some new results in the determination of crystallite size, *Journal of Applied Crystallography*, 11: 102-113.

Lopez-carrizales M., Pérez-díaz M.A., Mendoza-mendoza E., Peralta-rodríguez R.D., Ojeda-galván H.J., Portales-pérez D., Magaña-aquino M., Sánchez-sánchez R. and Martinez-

gutierrez F. (2022). Green, novel, and one-step synthesis of silver oxide nanoparticles: antimicrobial activity, synergism with antibiotics, and cytotoxic studies, *New Journal of Chemistry*, 46: 17841-17853.

Mushi N. (2023). Cellulose-Keratin Supramolecular Composite: Conformation by Combined Fourier Transform Spectroscopy and Partial Least Square Regression Coefficient, *Tanzania Journal of Engineering and Technology*, 42: 228-239.

Rosewald M., Hou F.Y.S., M mututuvari T., Harkins A. and D tran C. (2014). Cellulose-chitosan-keratin composite materials: synthesis, immunological and antibacterial properties, *ECS Transactions*, 64: 499.

Saxena I.M., Brown jr R.M. and Dandekar T. (2001). Structure–function characterization of cellulose synthase: relationship to other glycosyltransferases, *Phytochemistry*, 57: 1135-1148.

Shao W., Wang S., Wu J., Huang M., Liu H. and Min H. (2016). Synthesis and antimicrobial activity of copper nanoparticle loaded regenerated bacterial cellulose membranes, *RSC Advances*, 6: 65879-65884.

Singh S., Mohammad N., Pal K., Dhapte-pawar V., Saxena S. and Khanna P.K. (2024). Sonochemical synthesis of silver nanoparticles using orange juice: Cytotoxic behaviour and applications, *Hybrid Advances*, 6: 100220.

Somerville C. (2006). Cellulose synthesis in higher plants, Annu. Rev. Cell Dev. Biol., 22: 53-78. Taylor N.G. (2008). Cellulose biosynthesis and deposition in higher plants, *New Phytologist*, 178: 239-252.

Thanh N.T., Maclean N. and Mahiddine S. (2014). Mechanisms of nucleation and growth of nanoparticles in solution, *Chemical Reviews*, 114: 7610-7630.

Tran C.D., Makuwaza J., Munson E. and Bennett B. (2017). Biocompatible copper oxide nanoparticle composites from cellulose and chitosan: facile synthesis, unique structure, and antimicrobial activity, *ACS Applied Materials & Interfaces*, 9: 42503-42515.

Tran C.D., Prosenc F., Franko M. and Benzi G. (2016). One-pot synthesis of biocompatible silver nanoparticle composites from cellulose and keratin: characterization and antimicrobial activity, *ACS Applied Materials & Interfaces*, 8: 34791-34801.

Vishwanath R. and Negi B. (2021). Conventional and green methods of synthesis of silver nanoparticles and their antimicrobial properties, *Current Research in Green and Sustainable Chemistry*, 4: 100205.

Wang B., Yang W., Mckittrick J. and Meyers M.A. (2016). Keratin: Structure, mechanical properties, occurrence in biological organisms, and efforts at bioinspiration, *Progress in Materials Science*, 76: 229-318.

Wei L., Lu J., Xu H., Patel A., Chen Z.-S. and Chen G. (2015). Silver nanoparticles: synthesis, properties, and therapeutic applications, *Drug Discovery Today*, 20: 595-601.

Xia X., Zeng J., Zhang Q., Moran C.H. and Xia Y. (2012). Recent developments in shape-controlled synthesis of silver nanocrystals, *The Journal of Physical Chemistry C*, 116: 21647-21656.